Performance Evaluation and Security Analysis of UAV-Based FSO/CV-QKD System Employing DP-QPSK/CD

Nancy Alshaer , *Member, IEEE*, and Tawfik Ismail , *Senior Member, IEEE*

Abstract—Unmanned aerial vehicles (UAV) based on free-space optical (FSO) systems combine the benefits of both the high data rate of the FSO and the mobility of UAV. However, cumulative effects of laser beam divergence and turbulence-induced fading on the received irradiance in the FSO link might allow an external eavesdropper located near the authorized receiver to break the transmission under certain conditions. Quantum key distribution (QKD) is a technique of secure communication that employs quantum mechanics-based cryptography principles. A combination of a continuous-variable quantum key distribution (CV-QKD) and Gaussian modulation of quantum coherent states (GMCS) enables a relatively secure communication system against collective attacks over FSO transmission links. However, the performance is restricted and degraded due to the influence of atmospheric turbulence and excess noise. This paper aims to evaluate the performance of a secured UAV-based FSO system utilizing prepare and measure CV-QKD protocol based on GMCS under collective attack in terms of quantum bit error rate (QBER), outage probability, and secret key rate (SKR) considering the impairments of the FSO channel, link budget, deviations in the position and attitude angles of the UAV, channel fluctuating transmittance, and excess noise. The system parameters, including transmit power, receiver's field-of-view, and beam divergence angle, are optimized to satisfy the system's design criteria of threshold-QBER $= 10^{-3}$ and threshold outage probability $= 10^{-2}$. The proposed system tolerates boresight displacement up to 7 cm with the optimized values. The Closed-form expressions and analytical results are confirmed by Monte-Carlo simulations.

Index Terms—Continuous-variable quantum key distribution (CV-QKD), dual polarization quadrature phase shift keying (DP-QPSK), free-space optical (FSO), quantum coherent states (GMCS), performance evaluation, unmanned aerial vehicles (UAV).

I. INTRODUCTION

RECENTLY, secure and high-speed data transfer are major requirements for a variety of critical institutions such as,

financial and military. In contrast to conventional cryptography protocols whose security is based on theoretic assumptions of computational complexity, quantum key distribution (QKD) or quantum cryptography employs quantum mechanics physical laws such as, no-cloning theorem and Heisenberg uncertainty principle to achieve information-theoretic secure key exchange. These laws enable QKD to provide unconditional security, as quantum mechanics help to detect the existence of any adversary, usually named "Eve", during key exchange. Quantum cryptography solves the most difficult problem in modern cryptography, namely, key distribution. Once the key is generated it is subsequently utilized in a symmetric cipher, such as the one-time pad or one of the modern symmetric ciphers, to securely transmit information over a public classical authenticated channel [1], [2]. The quantum channel between the two remote entities who established the key, traditionally named Alice and Bob, can be optical fiber cable or free-space optical (FSO) channel [3], [4].

In FSO links the data transferred through the atmosphere faster than the glass in optical fiber cables that also suffers from polarization-preservation problem compared to the atmosphere that provides for almost unperturbed propagation of the polarization states. Furthermore, FSO links produce an alternative cost-effective communication to the places where optical fiber cannot be deployed [5], [6]. The FSO systems are based on intensity modulation with direct detection or coherent detection, which uses either homodyne or heterodyne detection. The motivation for using coherent FSO systems is that their receiver is limited only by the shot noise of the received light provided that the power of the optical local oscillator is sufficiently large. Consequently, coherent detection provides a means of overcoming thermal noise which can not be neglected due to harsh environmental conditions [7], [8]. In addition, coherent detection techniques support optical phase modulation formats as it converts phase variations into amplitude variations. The spectral efficiency of optical systems can be enhanced by exploiting dual polarization schemes that potentially duplicate the data rate compared to single polarization schemes [9], [10].

The usage of unmanned aerial vehicles (UAV), also known as drones, was primarily limited to military field. However, the improvement of advanced sensor implementation, flight control algorithms, and integrated circuit (IC) technology led to the development and design of UAVs of various sizes, and shapes that have advanced communication capabilities,

memory, storage, and onboard processing. Nowadays, UAVs have involved in a variety of commercial applications such as civilian, agriculture, disaster, rescue response, on-demand wireless systems with low-altitude, agent and multi-agent systems, and machine learning [11].

To take advantage of UAVs in wireless communication systems, it is essential to establish a data link between either UAV and existing networking infrastructures, UAV and newly constructed ground-control station (GCS), or UAV and UAV. The development of free-space communications technology motivates UAVs to perform applications including mapping, surveying, remote sensing, tracking, and traffic control. The UAV can either operate in a stationary mode or travel along a well-defined trajectory. Additionally, it can be easily integrated with current network infrastructures [12], [13]. Thus, the combination of UAV systems and FSO links is attracting attention due to the increased data rate as well as the license-free and secure transmission. Several commercial FSO links are deployed, which operate at 1–2 Gbps over ranges of 1–3 km [14], [15]. However, Atmospheric turbulence-induced fading, atmospheric attenuation, and pointing errors severely deteriorate the performance of terrestrial (fixed) FSO links [16], [17]. On the other hand, UAV-based FSO systems have another important factor limiting the reliability of the FSO link, namely, angle-of-arrival (AOA) fluctuations resulting from the orientation deviation of the hovering UAV.

In the literature, the channel model of a variety of configurations of UAV-based FSO links has been introduced [18]–[21]. A tractable channel model was proposed in [22] for the FSO link between UAVs under the effect of log-normal and Gamma-Gamma atmospheric turbulence beside considering the effects of atmospheric attenuation, geometric loss due to the deviation between the receiver lens center and the received beam center, and the link interruption due to AoA fluctuations. In addition, the closed-form expressions for the outage probability and bit error rate (BER) are derived. The performance of UAV-assisted FSO systems using an APD at the receiver was analyzed in [23]. Besides modeling end-to-end SNR of the considered FSO link and deriving closed-form expressions for the BER of the system under different turbulence conditions. Both [22] and [23] considered on-off keying (OOK) modulation and zero-boresight pointing errors. However, the system security has not been taken into consideration in the previous work.

In CV-QKD, the information is encoded into the amplitude or phase quadrature of the transmitted signal. The CV-QKD has attracted a great deal of attention as it offers the possibility of implementations using traditional telecommunications components. In addition, CV-QKD can utilize coherent detection techniques that operate more efficiently and faster than single-photon detectors used in discrete variable QKD (DV-QKD) protocol, enabling higher key distribution rates. Furthermore, a straightforward and cost-effective CV-QKD system has been achieved by using non-coherent detection techniques known as intensity modulation/direct detection (IM/DD) [24]. The CV-QKD systems appear to have the potential to accomplish two essential tasks. The first task is to refine the security analysis of CV-QKD protocols to take into account realistic concerns that occur during

their implementation stage. The second task is developing a practical mechanism that will allow these systems to achieve the high secret key rates that are theoretically presented in [25].

The CV-QKD protocols [26] were suggested on the basis of Gaussian modulation [27] of coherent [28] or squeezed states [29] employing either of heterodyne [30] or homodyne detection [31], [32]. Several experiments based on CV-QKD protocols have been successfully implemented over optical fiber [33], [34] or free space links [30]. The security of those protocols was analyzed regarding collective [35], individual [36], and coherent attacks [28]. The authors in [37] implemented a DV-QKD protocol (BB84) to enable the demonstration of a secure, high-speed optical communication data link between a drone and a ground station. In addition, size, weight, and power constraints related to the drone design have been considered such that a mass of 5 kg and power consumption of 20 W must not exceed. The performance of a secure ground-to-satellite FSO system has been evaluated in [38] employing CV-QKD protocol, taking into account the atmospheric channel attenuation, turbulence-induced scintillation, eye safety considerations, and the vertical beam link budget. The transmitter and receiver parameters such as bit rate, packet length, and scale coefficient step have been optimized in order to maximize the information capacity at the operating transmission distance.

An entanglement distribution has been demonstrated in [39] based on drones, realizing multi-weather operation including daytime and rainy nights. The system focused on a local-area network with 40 minutes and 200 m of on-demand coverage. Using a flying drone, an entanglement distribution has been accomplished in [40] where this mobile platform can be generalized for multiple mobile nodes with optical relay among them. Essential components for tracking, entangled source, and relay are developed with high performance.

In [41], an integrated system consisting of GCS, UAV, QKD, and FSO systems is introduced. The authors proposed a quantum key mechanism based on the E91 protocol combined with M-ary pulse position modulation (MPPM) with the time-bin technique to generate the secret key over the free space quantum channel considering the channel impairments. In addition to representing a channel model that study the combined effects of angle-of-arrival (AoA) fluctuations, nonzero boresight pointing error, atmospheric turbulence, and atmospheric attenuation. Furthermore, the variances in the position and orientation of the UAV are investigated using a tracking system. These variances are considered when evaluating the overall performance of the proposed integrated system.

As mentioned earlier, the researchers in the previous works are either concerned with the channel and system models, UAV tracking, or system security with QKD protocols and their immunity against possible attacks. This paper presents a comprehensive study of a secured ground-to-UAV FSO system using the CV-QKD protocol, including the design of the overall system, performance evaluation, parameter optimization, and vulnerability assessments. The proposed system prepares and measures CV-QKD protocol based on Gaussian modulated coherent states (GMCS) on a conventional FSO system utilizing Dual Polarization Quadrature Phase Shift Keying (DP-QPSK)

and coherent detection (CD) under collective attack. We assume that a tracking system is available that can precisely detect the location of the drone as well as its attitude angles. The combined impacts of the design parameters of the proposed integrated system are considered the main technical challenge of this research.

The key contributions are: (1) A model of the end-to-end SNR of a DP-QPSK with CD of a ground-to-UAV FSO link is deduced considering the effects of link budget and channel and receiver's excess noise. (2) Based on the developed analytical SNR model, analytical and closed-form expressions for the quantum bit error rate (QBER) and outage probability of the proposed system are derived. The effect of the whole channel state, including atmospheric attenuation, turbulence-induced scintillation, pointing errors, and AoA fluctuations of the hovering UAV, is embedded in these expressions. (3) Given the deduced QBER, the RKR and SKR expressions are introduced based on Shannon capacity limit and fluctuating transmittance. (4) Essential link parameters such as transmit power, receiver's field-of-view, and beam's divergence angle are optimized according to the design criteria of QBER, outage probability, UAV's position, and orientation deviations. (5) The analytical results and closed-form expressions are validated with the Monte Carlo simulations.

The remainder of this paper is organized in the following manner. The integration of the CV-QKD protocol over a UAV-based FSO system is described in Section II. The system model, including the transmitter, the receiver, and the quantum channel, is described in Section III. Section IV analyzes and evaluates the system performance in terms of QBER, outage probability, and SKR, as well as deriving closed-form expressions for QBER and outage probability. Additionally, the numerical results shown in Section V illustrate the validity of the derived expressions, which are used in conjunction with the optimized system parameters to demonstrate validity. Validation of the derived expressions is demonstrated via numerical results introduced in Section V in addition to the optimized system parameters. Finally, the proposed system and results are concluded in Section VI.

II. Integrated CV-QKD, FSO and UAV System

In order to integrate the QKD protocal with FSO and UAV systems, it is essential to describe the design of the quantum and public (classical) channels in free space. The quantum channel is a unidirectional optical channel from Alice to Bob. On the other hand, the public channel is a bidirectional optical channel between the two legitimate parts, namely, Alice and Bob.

The proposed system is presented in Fig. 1, where the GCS contains a dual-wavelength laser terminal that generates two-wavelengths λ_q and λ_u. A beam with λ_q for the quantum channel, while the other beam is with λ_u for the classical channel, both are from Alice (GCS) to Bob (UAV). These two optical beams are transmitting to the UAV, with the condition that the UAV QKD receiver must be isolated from the considerably stronger classical link received signal. The UAV has a laser source to provide the downlink (from Bob to Alice) classical channel at a wavelength of λ_d, which must be isolated from the UAV QKD receiver. The selection of the appropriate wavelength is critical,
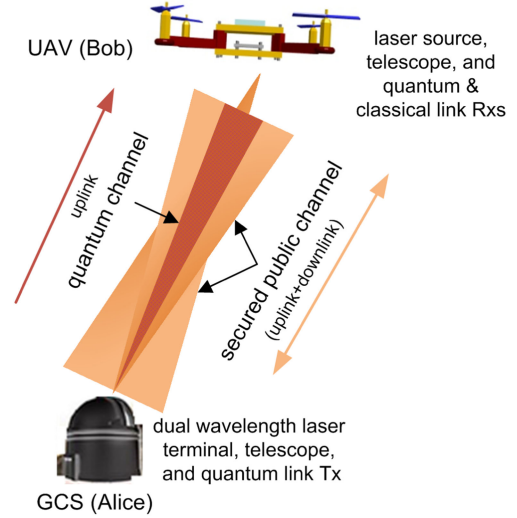

Fig. 1. System layout and channels. GCS: ground control station; UAV: unmanned Unmanned aerial vehicle.

and wavelength selective filters are the major isolation method. Notch filters will also be used at the UAV to distinguish between the three wavelengths.

In the proposed system, the secure keys (symbols/sec) are sent via the quantum channel using a DP-QPSK/CD transmitter, allowing higher quantum key rates than direct detection (DD) systems. The coherent optical detector detects the symbols at Bob's side. The detected key is then resent again to Alice through the downlink channel for approval. This downlink is also used to transmit the channel state information (CSI) from Bob to Alice for the reconciliation process. The receiver accurately estimates the instantaneous channel's fading state and inserts pilot symbols at the beginning of a block of symbols. Alice receives Bob's bits and determines the QBER using an offline version of the originally transmitted bits. She utilizes the CSI and QBER to discover Eve's existence. If not, the secret key is sent through the uplink public channel. Finally, the encrypted data is also transmitted via the public channel.

In an eavesdropping attack, Eve should also be a UAV who suffers from Bob's same challenging issues when locating herself close to Bob. This is a novel security situation completely different from a traditional scenario with Eve in a fixed position. She must also maintain a safe distance from Bob to avoid crashing with Bob due to random hovering, but she must remain within the beam footprint to receive a signal. The relative distance between Eve and Bob concerning the random misalignments of the beam centroid should have a considerable impact on the possible SKR, especially when pointing errors in the legitimate links are assumed. This practical issue is out of the scope of the current framework of this paper, and we assumed that Eve has a mechanism that keeps her close to Bob and avoid collision with him.

III. System Model

This work considers an FSO system with DP-QPSK modulation and optical coherent-detection. The proposed system is
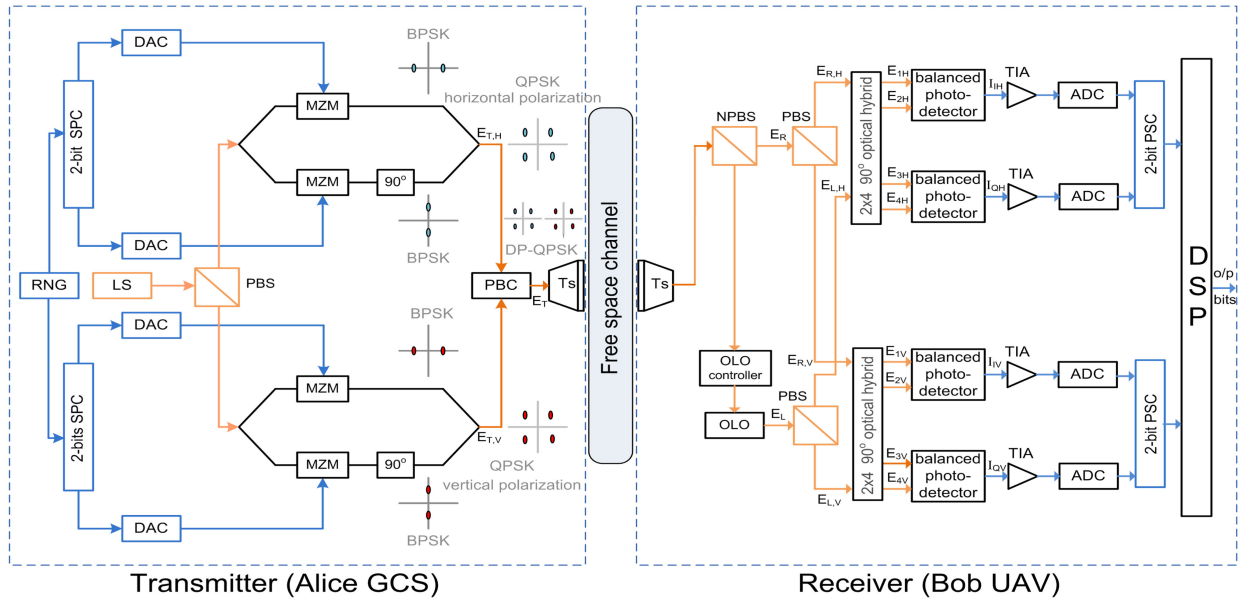
Fig. 2. A block diagram of the proposed free space CV-QKD system using DP-QPSK/CD. RNG: random number generator; DAC: digital-to-analog converter; LS: laser source; SPC: serial parallel converter; PBS: polarizing beam splitter; MZM: Mach-Zehnder modulator; BPSK: binary phase shift keying; QPSK: quadrature phase shift keying; PBC: polarizing beam combiner; Ts: telescope; GCS: ground control station; NPBS: non-polarizing beam splitter; OLO: optical local oscillator; TIA: transimpedance amplifier; ADC: analog-to-digital converter; PSC: parallel-to-serial converter; UAV: unmanned aerial vehicle; DSP: digital signal processor.

shown in Fig. 2. It consists of three essential subsystems: the transmitter (Alice), the receiver (Bob), and the wireless channel.

A. The Transmitter

The sequence of random bits produced by Alice is generated with a random number generator (RNG). She uses an optical Mach-Zehnder modulator (MZM), in push-pull regime, with the $90°$ phase-shift to construct QPSK modulation. In order to develop DP-QPSK, a polarizing beam splitter (PBS) is used to split the light produced by the laser source λ_q into two orthogonality polarized beams, vertical (V) and horizontal (H). In contrast, each polarized light carries a QPSK symbol $b(t)$. The outputs of each modulator with V and H polarization are combined before being transmitted over the FSO channel. The output of the combined optical signal to be transmitted is expressed as:

$$E_{T,H}(t) = \sqrt{2\,P_{T,H}}\; e^{j(\omega_q t + \phi_s(t))}\, |b_H(t)| e^{j\phi(t)},$$
$$E_{T,V}(t) = \sqrt{2\,P_{T,V}}\; e^{j(\omega_q t + \phi_s(t))}\, |b_V(t)| e^{j\phi(t)},$$
$$E_T(t) = E_{T,H}(t) + E_{T,V}(t), \qquad (1)$$

where $P_{T,V}, P_{T,H}$ represent the transmit power vertically and horizontally polarized. The angular frequency and optical signal phase are expressed by ω_q and ϕ_s, respectively. The modulating signal from the DAC has the amplitude and phase $|b(t)|$ and $\phi(t)$. A polarizing beam combiner (PBC) is used to combine the two signals at the outputs of the upper and lower IQ modulators, $E_{T,H}(t)$ and $E_{T,V}(t)$, to display the DP-QPSK signal $E_T(t)$.

B. The Receiver

The receiver uses a coherent detection approach in order to recover the transmitted data. Coherent detection refers to the ability of an optical receiver to track the phase of an optical

transmitter in order to extract the phase information carried by a transmitted signal. In the coherent detection, the receiver calculates a decision variable by measuring the phase difference between the desired signal and a reference phase from an optical local-oscillator (OLO) in order to recover information from both the I and Q components of an optical carrier. The optical field associated with the local oscillator for horizontal or vertical polarized components is given by

$$E_L(t) = \sqrt{2\,P_L}\; e^{j(\omega_L t + \phi_L(t))}, \qquad (2)$$

where P_L, ω_L, and ϕ_L are the power, the angular frequency, and the phase of the OLO, respectively.

The incident optical field at the input of each PBS is made up of two components: the received modulated carrier $E_R(t) = hE_T(t)$ where h is the channel state, and the optical local oscillator $E_L(t)$, which are orthogonal polarized. The resulting orthogonal polarization components are fed into two IQ demodulators to recover the signal $b(t)$. Each IQ demodulator consists of a six-port $90°$ optical hybrid and a pair of balanced photo-detectors (BPDs). The $90°$ optical hybrid introduces a $90°$ phase shift between I and Q components and a $180°$ phase shift between the BPDs. The six-port $90°$ optical hybrid with two input $E_{R,H}$ and $E_{L,H}$ from the PBS has four output signals E_{1H-4H} [42]. The balanced configuration of the photo-detectors, two detectors with outputs fed into a differential amplifier uses to block the common mode components such as the DC components, the relative intensity noise (RIN), and the amplified spontaneous emission (ASE) noise.

In horizontally H polarized signal, the first BPD output introduces the in-phase component I_{IH} while the second BPD output introduces the quadrature-phase component I_{QH}. The

photocurrents of I_{IH} and I_{QH} are given by [43], [44]:

$$I_{IH} = 2\Re\sqrt{P_R P_L}\,|b_H(t)|\,\mathbf{e}_s\mathbf{e}_l\cos[\omega_{IF}t + \Delta\phi(t) + \phi(t)],$$

$$I_{QH} = 2\Re\sqrt{P_R P_L}|b_H(t)|\mathbf{e}_s\mathbf{e}_l\sin[\omega_{IF}t + \Delta\phi(t) + \phi(t)],$$

(3)

where P_R is the received optical power, $\mathbf{e}_s$ and $\mathbf{e}_l$ are the polarization unit vectors of $E_{R,H}$ and $E_{L,H}$. $\Re$ is the responsivity of the photo-detector, ω_{IF} is the angular frequency difference $(\omega_q - \omega_L)$, and $\Delta\phi(t)$ is the time-varying phase difference $(\phi_s(t) - \phi_L(t))$. The received optical power P_R, for vertical or horizontal polarized components, can be expressed as a function of the overall channel state h by [45], [46]:

$$P_R(h) = P_T\,\eta_T\,\eta_R\,G_T\,G_R\left(\frac{\lambda}{4\pi L}\right)^2 h,$$

(4)

where η_T, η_R, $G_T = (\pi D_T/\lambda)^2$, and $G_R = (\pi D_R/\lambda)^2$ are the optical efficiencies and the telescope gains of the Tx and the Rx, respectively. D_T is the Tx aperture diameter, and D_R is the Rx aperture diameter. L is the transmission distance, and λ is the laser wavelength. In addition, the P_R uses to control the output of OLO power such that the condition of $P_L \gg P_R$ should be satisfied.

Similarly, in vertically V polarized signal, the first BPD output introduces the in-phase component I_{IV} while the second BPD output introduces the quadrature-phase component I_{QV}. The photocurrents of I_{IV} and I_{QV} are given by :

$$I_{IV} = 2\Re\sqrt{P_R P_L}\,|b_V(t)|\,\mathbf{e}_s\mathbf{e}_l\cos[\omega_{IF}t + \Delta\phi(t) + \phi(t)],$$

$$I_{QV} = 2\Re\sqrt{P_R P_L}|b_V(t)|\mathbf{e}_s\mathbf{e}_l\sin[\omega_{IF}t + \Delta\phi(t) + \phi(t)].$$

(5)

Those photocurrents are amplified with trans-impedance amplifiers (TIA) to achieve high sensitivity and wide bandwidth before arriving at the analog-to-digital converters (ADC). The signal is then processed by a digital signal processor (DSP) to maximize the mutual information between Alice and Bob. Furthermore, the outputs of carrier phase estimation (CPE) and carrier frequency estimation (CFE) control the local oscillator, enabling the phase and frequency of the output laser to be digitally locked to the received optical signal. Finally, symbols (bits) sent over the channel are detected by a symbol detector, which slices the received constellation using appropriate thresholds. Suppose Alice and Bob fail to observe an Eve. The detected symbols (output bits) obtained at the DSP output are then used to establish the secret key [47]–[49].

C. Free-Space Channel Model

The overall channel state h of the FSO link combines the effects of four independent components h_l, h_t, h_p, and h_a. The first component is the atmospheric attenuation h_l that is represented by Beer-Lambert law as a function of the atmospheric attenuation coefficient, and the link distance [50]. The second component is the atmospheric turbulence h_t resulting from random fluctuations in the pressure and temperature of the atmosphere and can be interpreted by several mathematical

models based on its intensity [16], [51]. The third component is the pointing error h_p that occurs as a result of misalignment between the beam and detector centers [17], where the radial displacement between them follows the Beckmann distribution [52]. Finally, the fourth factor is the link interruption h_a caused by the fluctuations in the angle-of-arrival (AoA) [21]. Thus, the probability density function (PDF) of the channel state h for ground-to-UAV link includes the four state components h_l, h_t, h_p, and h_a is given by [21]:

$$f_h(h) = \exp\left(\frac{-\theta_{FoV}^2}{2\sigma_o^2}\right)\delta(h) + \left[1 - \exp\left(\frac{-\theta_{FoV}^2}{2\sigma_o^2}\right)\right]$$

$$\times \sum_{j=0}^{J}\frac{1}{j!}\left(\frac{\alpha\beta}{A_0 h_l}\right)^j\left(v_j(\alpha,\beta)h^{\beta-1+j} - v_j(\beta,\alpha)h^{\alpha-1+j}\right),$$

(6)

where $v_j(\alpha,\beta)$ and $v_j(\beta,\alpha)$ are given in [53] for the general case of nonzero boresight pointing errors as following

$$v_j(\alpha,\beta) = \frac{\pi\gamma^2\left(\frac{\alpha\beta}{A_0 h_l}\right)^\beta[\sin((\alpha-\beta)\pi)]^{-1}}{\Gamma(\alpha)\Gamma(\beta)\Gamma(j-(\alpha-\beta)+1)|-(\beta-\gamma^2+j)|}$$

$$\times \exp\left(\frac{-s^2}{2\sigma_{pg}^2} - \frac{s^2\gamma^2/\sigma_{pg}^2}{2\beta - 2\gamma^2 + 2j}\right),$$

(7)

and

$$v_j(\beta,\alpha) = \frac{\pi\gamma^2\left(\frac{\alpha\beta}{A_0 h_l}\right)^\alpha[\sin((\beta-\alpha)\pi)]^{-1}}{\Gamma(\alpha)\Gamma(\beta)\Gamma(j+(\alpha-\beta)+1)|-(\alpha-\gamma^2+j)|}$$

$$\times \exp\left(\frac{-s^2}{2\sigma_{pg}^2} - \frac{s^2\gamma^2/\sigma_{pg}^2}{2\alpha - 2\gamma^2 + 2j}\right),$$

(8)

A_0 is a fraction of power collected at $r = 0$, $A_0 = [\mathrm{erf}(\nu)]^2$, where r is the radial displacement between the beam center and the photodetector (PD) center [[17], Fig. 2]. The erf(.) is the standard error function, $\mathrm{erf}(x) = 2/\sqrt{\pi}\int_0^x \exp(-t^2)\,dt$. And the ratio between the aperture radius of the receiver r_a and the beam waist ω_z at distance z is $\nu = \sqrt{\pi/2}(r_a/\omega_z)$. α and β are the effective number of large-scale and small-scale turbulence eddies, respectively. They are directly related to the atmospheric conditions [54]. θ_{FoV} is the field-of-view (FoV) angle of the receiver. J is defined as $\lfloor J = \gamma^2 - \alpha\rfloor$, $\gamma = \omega_{zeq}/2\sigma_{pg}$ is the ratio between the equivalent beamwidth, $\omega_{zeq}^2 = \omega_z^2(\sqrt{\pi}\mathrm{erf}(\nu)/2\nu\exp(-\nu^2))$ and jitter standard deviation measures the pointing error severity [53]. The radial displacement $r = |\mathbf{r}| = \sqrt{r_x^2 + r_y^2 + r_z^2}$ [52], where r_x, r_y, and r_z are modeled as nonzero mean Gaussian distributed independent RVs with means μ_x, μ_y, and μ_z, respectively [53]. In addtion to the random jitters, the nonzero boresight errors are considered here where the boresight displacement s is given by $s = \sqrt{\mu_x^2 + \mu_y^2 + \mu_z^2}$.

σ_o^2 is the variance of the orientation deviation of the UAV is given by: $\sigma_o^2 = \sigma_\theta^2 + \sigma_\phi^2 + \sigma_\psi^2$ where σ_θ^2, σ_ϕ^2, and σ_ψ^2 are the attitude variances calculated by the pitch (θ), the roll (ϕ), and the
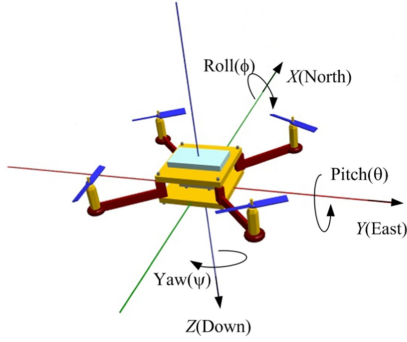
Fig. 3. Position and attitude coordinates of the UAV.

yaw (ψ) orientation angles as presented in Fig. 3. Furthermore, σ_{pg}^2 is the variance of position deviation between UAV and GCS, $\sigma_{pg}^2 = \sigma_p^2 + \sigma_g^2$, where σ_g^2 is the variance of GCS position fluctuations while σ_p^2 is the variance of position deviation of the UAV is given by: $\sigma_p^2 = \sigma_x^2 + \sigma_y^2 + \sigma_z^2$ where σ_x^2, σ_y^2, and σ_z^2 are the position variances in x, y, and z directions, respectively.

D. Gaussian-Modulated Coherent States

A well-known approach that has been demonstrated to be robustly used against collective attacks is the CV-QKD technique that utilizes Gaussian-modulated coherent states (GMCS). Currently, various research groups are implementing CV-QKD-based GMCS techniques in both the experimentally and in the field [55]–[57]. Fig. 4 illustrates the GMCS integrated with CV-QKD over FSO channel. In GMCS, Alice modulates the quadrature of coherent states using Gaussian modulation and sends it to Bob via the quantum channel (free space). The atmospheric channel is characterized by a fluctuating transmittance T of probability distribution $\tau(T)$ with mean $\langle T \rangle$, given as [[58], (2)], and an excess noise ε_{ch}, resulting in a noise variance of $(1 + \langle T \rangle \varepsilon_{ch})$ at Bob's input. The total channel-added noise that is referred to as channel input, expressed in shot noise units, is given by [59]

$$\chi_{line} = \frac{1 + \langle T \rangle \varepsilon_{ch}}{\langle T \rangle} - 1 = \frac{1}{\langle T \rangle} + \varepsilon_{ch} - 1 . \quad (9)$$

The modulated coherent states received by Bob are detected using homodyne detector that measures either one of the two quadratures using heterodyne detector to measure both quadratures simultaneously to obtain the secret key. The imperfection of the detector is described by the electronic noise v_{el} and the detection efficiency η. A detection-added shot-noise units for heterodyne detection at Bob is $\chi_h = 2 \times ((1 - \eta) + v_{el})/\eta$. Therefore, the total noise referred to the channel input could be expressed as [60]

$$\chi_{tot} = \chi_{line} + \frac{\chi_h}{\langle T \rangle}. \quad (10)$$

Beyond the unavoidable shot noise, various practical imperfection will contribute to the total noise and deteriorate the performance of the system. In a typical CV-QKD system, the three terms that contribute significantly to the excess noise [[61], Fig. 4] are detection noise ε_{det}, the quantization noise ε_{ADC},

and the imperfect phase recovery noise ε_{PR}. All those noise sources are assumed to be stochastically independent, so the variances they cause to the quadratures are additive. The excess noise ε is divided into two main parts, one part originating from the free space quantum channel ε_{ch} and another part related to the receiver $\varepsilon_{rec} = \varepsilon_{det} + \varepsilon_{ADC} + \varepsilon_{PR}$, where its components are defined in [61]. In this paper, we assume that Eve does not have access to Bob's detection apparatus. Therefore, the receiver added noise (excess noise) would not contribute to the Holevo information. However, it still affects the results of Bob's measurements and hence the signal-to-noise ratio and mutual information, as will be declared in detail through the next section.

IV. PERFORMANCE ANALYSIS AND EVALUATION

The performance of a QKD-based FSO system is usually evaluated in terms of QBER, secret key-rate (SKR), and outage probability (P_{out}). In this section, closed-form expressions of QBER and the outage probability of the proposed integrated system are presented using a QPSK modulation scheme with coherent detection. In addition to introducing an exact form of the secret key rate.

A. Quantum Bit Error Rate Analysis

QBER for the CV-QKD protocol over FSO link with instantaneous BER $P_e(h)$ and PDF $f_h(h)$ can be written as

$$\text{QBER} = \int_0^\infty P_e(h) f_h(h) dh, \quad (11)$$

where the instantaneous BER of the QPSK modulation scheme for a given channel state h could be expressed as [62]:

$$P_e(h) = \frac{1}{2} \text{erfc} \left(\sqrt{\text{SNR}} \, h \right), \quad (12)$$

where erfc(.) is the complementary error function. The average signal-to-noise ratio $\overline{\text{SNR}}$ is defined as [10]:

$$\overline{\text{SNR}} = \frac{\hat{I}^2}{2\sigma_n^2}, \quad (13)$$

where $\hat{I}$ is the expectation of the photocurrent at the output of the BPD due to horizontally polarized signal (3) or vertically polarized signal (5). σ_n^2 is Gaussian noise of zero mean and variance, $\sigma_n^2 = \sigma_s^2(1 + \eta \langle T \rangle \varepsilon + v_{el}) + \sigma_b^2 + \sigma_{th}^2$, where σ_s^2, σ_b^2, and σ_{th}^2 are the shot noise, the background noise, and the thermal noise variances, respectively [22], [59].

By substituting (6) and (12) in (11) the QBER is can be expressed as:

$$\text{QBER} = \frac{1}{2} \int_0^\infty \text{erfc} \left(\sqrt{\text{SNR}} \, h \right) \times \left[\exp \left(\frac{-\theta_{FoV}^2}{2\sigma_o^2} \right) \delta(h) \right.$$

$$+ \left[1 - \exp \left(\frac{-\theta_{FoV}^2}{2\sigma_o^2} \right) \right] \times \sum_{j=0}^J \frac{1}{j!} \left(\frac{\alpha\beta}{A_0 h_l} \right)^j$$

$$\left. \left(v_j(\alpha, \beta) h^{\beta-1+j} - v_j(\beta, \alpha) h^{\alpha-1+j} \right) \right] dh. \quad (14)$$
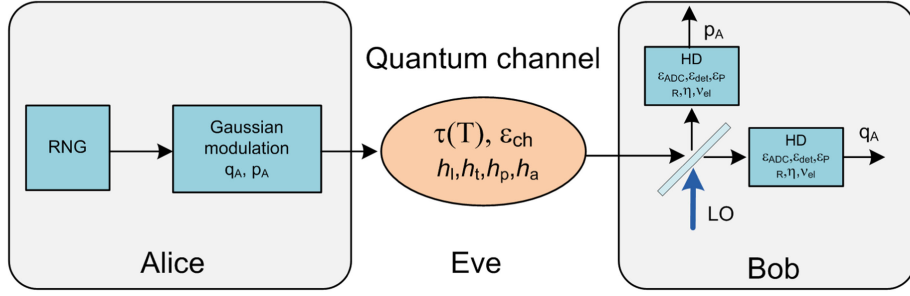
Fig. 4. Description of prepare and measure CV-QKD relying on GMCS and heterodyne detection over FSO channel. The quantum channel has fluctuating transmittance T governed by a probability distribution $\tau(T)$ and excess channel noise ε_{ch}. Alice modulates (prepares) coherent light states through randomly selecting two values for the in-phase quadrature q_A and the orthogonal quadrature p_A follow a Gaussian distribution. Eve has access to the quantum channel (through controlling T and ε_{ch}) but not to the apparatuses in Bob's lab. The detector imperfection is described by the detection efficiency η and the electronic noise v_{el}. RNG: random number generator; BS: beam splitter; LO: local oscillator; HD: homodyne detection; h_l: atmospheric attenuation; h_t: atmospheric turbulence; h_p: pointing error (transceiver misalignment); and h_a: link interruption due to AoA fluctuations.

The closed-form expression of the QBER could be extracted by using [[63], (06.27.21.0132.01)], as:

$$\text{QBER} = \frac{1}{2}\left[\exp\left(\frac{-\theta_{FoV}^2}{2\sigma_o^2}\right)\right]$$

$$+ \frac{M-1}{2\sqrt{\pi}}\left[1 - \exp\left(\frac{-\theta_{FoV}^2}{2\sigma_o^2}\right)\right]\sum_{j=0}^{J}\frac{1}{j!}\left(\frac{\alpha\beta}{A_0 h_l}\right)^j$$

$$\times \left[\frac{\Gamma(\frac{\beta+j+1}{2})}{\beta+j}\left(\sqrt{\text{SNR}}\right)^{-(\beta+j)} v_j(\alpha,\beta)\right.$$

$$\left. - \frac{\Gamma(\frac{\alpha+j+1}{2})}{\alpha+j}\left(\sqrt{\text{SNR}}\right)^{-(\alpha+j)} v_j(\beta,\alpha)\right]. \quad (15)$$

B. Secret Key-Rate Analysis

An eavesdropper Eve is presumed to be the cause of both losses and noise within the channel. She can obtain and store information about signal states. However, she is limited in her attacks on the quantum channel due to the laws of physics. Bob, on his side, conducts a heterodyne measurement with an auxiliary LO and proceeds to key sifting, error correction, and privacy amplification using an authenticated classical channel established beforehand with Alice. After Alice and Bob share a sequence of states, they will expose and compare a subset of the data sent as well as the accompanying measurements. It is possible to estimate the overall transmission and excess noise of the channel by analyzing them, and it is from this estimate that they can determine their sifting or secret key rate. If the mutual information between Alice and Bob less than the information received by Eve, the protocol should abort the connection and hence no secret key can be distilled [58]. The asymptotic raw key rate (RKR) and secret key rate (SKR) of the CV-QKD protocol can be calculated by [59], [61]:

$$\text{RKR} = (1 - \text{QBER})(\langle T \rangle \beta_R I_{AB}),$$

$$\text{SKR} = (1 - \text{QBER})(\langle T \rangle \beta_R I_{AB} - \chi_{BE}), \quad (16)$$

where I_{AB} is the mutual information between Alice and Bob (upper-bounded by the channel capacity/Shannon limit) and

χ_{BE} is the Holevo quantity that represents the limit of the maximum information on Bob's key available to Eve in the case of collective attack. β_R is the reconciliation efficiency. The information reconciliation of the proposed system is reverse reconciliation (RR) as Alice corrects her bits according to Bob's data, i.e., Bob agrees to be the reference side of the protocol [58], [61]. In order to calculate the Holevo quantity, a covariance matrix γ_{AB} should be presented. It describes the shared state after traveling through an untrusted channel and received by Bob. The covariance matrix γ_{AB} can be expressed as [59], [60]:

$$\gamma_{AB} = \begin{pmatrix} V\| & \langle\sqrt{T}\rangle\sqrt{V^2-1}\sigma_z \\ \langle\sqrt{T}\rangle\sqrt{V^2-1}\sigma_z & \langle T\rangle(V+\chi_{line})\| \end{pmatrix}, \quad (17)$$

where $V = V_A + 1$, and V_A is the modulation variance. σ_z is the 2×2 Pauli matrix and $\|$ is the 2×2 identity matrix. Therefore, the Holevo quantity χ_{BE} could be calculated by [60]:

$$\chi_{BE} = \sum_{i=1}^{2} G\left(\frac{\lambda_i - 1}{2}\right) - \sum_{i=3}^{5} G\left(\frac{\lambda_i - 1}{2}\right), \quad (18)$$

where $G(x) = (x+1)\log_2(x+1) - x\log_2 x$. The five symplectic eigenvalues λ_{1-5} are expressed in [59]. Finally, the Shannon capacity limit which maps I_{AB} over the quantum channel with PDF $f_h(h)$ expressed in (6), is derived as [46], [64]:

$$I_{AB} = \int_0^\infty \log_2(1 + \overline{\text{SNR}}\, h^2) f_h(h)\, dh. \quad (19)$$

Hence the SKR in (16) is obtained as a function of the quantum channel PDF, which is related to the channel state h (combined of h_t, h_l, h_p, and h_a) and includes essential system parameters such as SD of orientation and position deviations. Also, SKR is a function of the average signal-to-noise ratio given in (13) which impacts the effects of detection efficiency, excess noise, and mean channel transmittance.

C. Outage Probability Analysis

The outage probability P_{out} is an important performance metric for the QKD quantum channel. It is defined as the probability that the instantaneous signal-to-noise ratio SNR(h) falls below a

dedicated threshold SNR_{th}. This threshold should keep the SKR presented in (16) greater than zero, i.e. ($\langle T \rangle \, \beta_R \, I_{AB} > \chi_{BE}$). The P_{out} could be expressed as [46]:

$$P_{\text{out}} = P_r(\text{SNR}(h) < \text{SNR}_{th}) = \int_0^{\varepsilon_o} f_h(h); \, dh, \quad (20)$$

where $\varepsilon_o = \sqrt{\text{SNR}_{th}/\overline{\text{SNR}}}$. Substituting (6) into (20), the outage probability is given by

$$P_{\text{out}} = \int_0^{\varepsilon_o} \exp\left(\frac{-\theta_{FoV}^2}{2\sigma_o^2}\right) \delta(h) \, dh + \left[1 - \exp\left(\frac{-\theta_{FoV}^2}{2\sigma_o^2}\right)\right]$$
$$\times \sum_{j=0}^{J} \frac{1}{j!}\left(\frac{\alpha\beta}{A_0 h_l}\right)^j$$
$$\times \int_0^{\varepsilon_o} \left[\left(v_j(\alpha,\beta)h^{\beta-1+j} - v_j(\beta,\alpha)h^{\alpha-1+j}\right)\right] dh. \quad (21)$$

The integration in the first part of (21) is solved as [21]:

$$\int_0^{\varepsilon_o} \exp\left(\frac{-\theta_{FoV}^2}{2\sigma_o^2}\right)\delta(h)\,dh = \exp\left(\frac{-\theta_{FoV}^2}{2\sigma_o^2}\right)\int_0^{\varepsilon_o}\delta(h)\,dh$$
$$= \exp\left(\frac{-\theta_{FoV}^2}{2\sigma_o^2}\right). \quad (22)$$

From (7) and (8) both the terms $v_j(\alpha,\beta)$ and $v_j(\beta,\alpha)$ are independent of h. So, the integral in the second part of (21) is solved using the simple integral rule, $\int_0^b y^a \, dy = b^{a+1}/(a+1)$. Where $y = h$, $b = \varepsilon_o$, and $a = (\beta - 1 + j)$ or $(\alpha - 1 + j)$. So, the integral is calculated as:

$$\int_0^{\varepsilon_o}\left[\left(v_j(\alpha,\beta)h^{\beta-1+j} - v_j(\beta,\alpha)h^{\alpha-1+j}\right)\right]dh.$$
$$= \left[\left(v_j(\alpha,\beta)\varepsilon_o^{\beta+j}/(\beta+j) - v_j(\beta,\alpha)\varepsilon_o^{\alpha+j}/(\alpha+j)\right)\right]. \quad (23)$$

The closed-form expression for P_{out} is obtained as:

$$P_{\text{out}} = \left[\exp\left(\frac{-\theta_{FoV}^2}{2\sigma_o^2}\right)\right] + \left[1 - \exp\left(\frac{-\theta_{FoV}^2}{2\sigma_o^2}\right)\right]$$
$$\times \frac{\exp(\frac{-s^2}{2\sigma_{pg}^2})\pi\gamma^2}{\Gamma(\alpha)\Gamma(\beta)\sin(\pi(\alpha-\beta))}\sum_{j=0}^{J}\left(\frac{\alpha\beta}{A_0 h_l}\right)^j$$
$$\times \left[\frac{\left(\frac{\alpha\beta}{A_0 h_l}\right)^\beta \exp(-\frac{s^2\gamma^2/\sigma_{pg}^2}{2\beta-2\gamma^2+2j})\,\varepsilon_o^{(\beta+j)}}{(\beta+j)\Gamma(j-(\alpha-\beta)+1)|-(\beta-\gamma^2+j)|}\right.$$
$$\left. - \frac{\left(\frac{\alpha\beta}{A_0 h_l}\right)^\alpha \exp(-\frac{s^2\gamma^2/\sigma_{pg}^2}{2\alpha-2\gamma^2+2j})\,\varepsilon_o^{(\alpha+j)}}{(\alpha+j)\Gamma(j+(\alpha-\beta)+1)|-(\alpha-\gamma^2+j)|}\right], \quad (24)$$

where (7) and (8) are rewritten using the exponential rule $\exp(x-y) = \exp(x)\,\exp(-y)$.

TABLE I
FSO COMMUNICATION SYSTEM AND CHANNEL PARAMETERS

Parameter	Symbol	Value
System Parameters		
UAV altitude	L	500 m
QBER threshold	QBER_{th}	10^{-3}
Outage probability threshold	$P_{\text{out-th}}$	10^{-2}
Threshold SNR	SNR_{th}	5 dB
Transmitter diameter	D_T	0.1 m
Receiver diameter	D_R	0.1 m
Wavelength	λ	1550 nm
Optical transmit power	P_T	0 to 10 dBm
Reconciliation efficiency	β_R	0.9
Detection efficiency	η	0.75
Detector responsivity	$\Re$	0.5 A/W
Modulation variance	V_A	6 SNU
Excess noise	ε	0.065 SNU
Electronic noise	v_{el}	0.01 SNU
Local-oscillator power	P_L	10.7 to 20.7 dBm
Electrical bandwidth	B_e	250 MHz
Optical bandwidth of the LO	B_o	10 kHz
Beamwidth at the receiver	w_z	37.96 cm
Channel Parameters		
Rytov variance	σ_R^2	2
Effective number of large-scale cells	α	3.9927
Effective number of small-scale cells	β	1.7206
Mean channel transmittance	$\langle T \rangle$	0.6, 0.9
Atmospheric attenuation coefficient	β_l	13.8 dB/km

V. SIMULATION RESULTS AND DISCUSSION

We adopt an atmospheric transmittance probability distribution with an elliptic-beam approximation to simulate the transmittance in the FSO link with varied parameters. The model is based on the assumption of a Gaussian optical beam propagating through the atmospheric link with isotropic turbulence, where the beam is distorted and subjected to atmospheric loss, pointing errors, turbulence-induced fading caused by atmospheric conditions, and AoA fluctuations, as well as eavesdropping collective attack. The simulation aims to optimize the system parameters such as beam's divergence angle and receiver's field-of-view to keep the QBER below a certain threshold QBER_{th}, assumed to be 10^{-3}, and the outage probability below a threshold $P_{\text{out-th}}$ of 10^{-2} which in turn helps to maximize the secret key rate [64]. This will be accomplished using expressions deduced in Section IV for the QBER, SKR, and the outage probability. The simulation has carried out using MathWorks-MATLAB-2021 A and the Monte Carlo simulation has been developed in order to verify the accuracy of the derived expressions. Given the random nature of air turbulence, we executed 1000 iterations of the Monte Carlo turbulence method for each given communication distance to confirm that our results were accurate. System parameters are summarized in Table I based on recent researches [22], [59], [61].

As shown in Fig. 5, the QBER of the proposed system is calculated for transmit power (P_T) ranging from 0 to 10 dBm, receiver's field-of-view ($\theta_{\text{FoV}} = 15$ and 20 mrad) and beam's divergence angle ($\theta_{\text{div}} = 1.5$ and 2.5 mrad). It is apparent that QBER $< 10^{-3}$ is realized for $\theta_{\text{FoV}} = 20$ mrad in two cases: the first case when $P_T > 9$ dBm and $\theta_{\text{div}} = 2.5$ mrad, and the second case when $P_T > 3$ dBm and $\theta_{\text{div}} = 1.5$ mrad. Furthermore, the results of the proposed driven closed-form expression of the QBER, as well as the simulated results presented in Fig. 5, prove
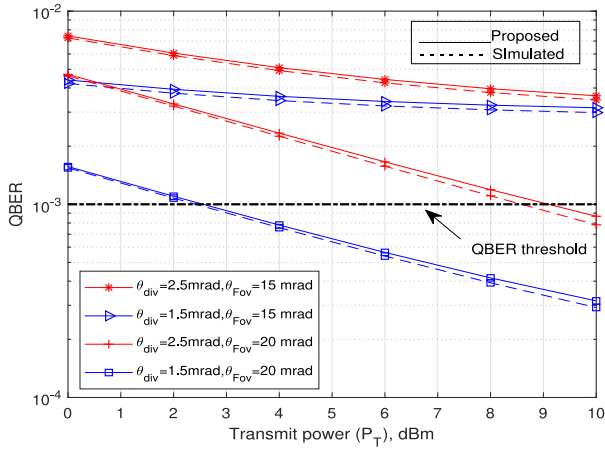
Fig. 5. QBER as versus transmit power for (θ_{div} = 1.5 mrad and 2.5 mrad) and (θ_{FoV} = 15 mrad and 20 mrad).

Fig. 7. QBER versus receiver's field-of-view for θ_{div}=1.5 mrad and P_T =4 dBm and different UAV position and orientation SD.
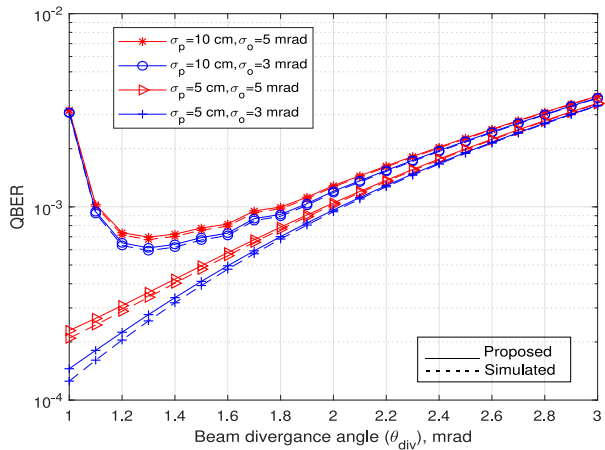

Fig. 6. QBER versus beam divergence angle for θ_{FoV}=20 mrad and P_T=4 dBm and different UAV position and orientation SD.

Fig. 8. QBER as a function of the normalized boresight for σ_p=10 cm, σ_o=5 mrad, P_T=4 dBm, θ_{div}=1.5 mrad, and θ_{Fov}=20 mrad.

a perfect matching, and hence the driven expression of the QBER is trusted.

As a consequence of the results obtained by Fig. 5, we considered that θ_{FoV} and P_T are set to be 20 mrad and 4 dBm, respectively. Accordingly, we extend our study to determine the most appropriate value for θ_{div}. Therefore, Fig. 6 presents the effect of changing θ_{div} from 1 to 2 mrad on the QBER, which takes into account the fluctuation in the standard deviation of position and orientation with the tracking system accuracy. According to Fig. 6, 1.1 mrad $< \theta_{\mathrm{div}} <$ 1.7 mrad guarantees QBER $<$ QBER$_{\mathrm{th}}$ for position SD σ_p = 5 and 10 cm, and orientation SD σ_o = 3 and 5 mrad. Accordingly, the value of θ_{div} is set to 1.5 mrad in the following results as a result of the preceding decision.

Fig. 7 is presented in order to investigate the impact of varying the receiver field of view θ_{FoV} on the QBER. It shows the quantified response of the QBER as a function of θ_{FoV} varying from 10 to 25 mrad while taking into consideration the variance in the UAV position and orientation. As can be shown, the system performance is stable in terms of the QBER for $\theta_{\mathrm{FoV}} \geq$ 20 mrad
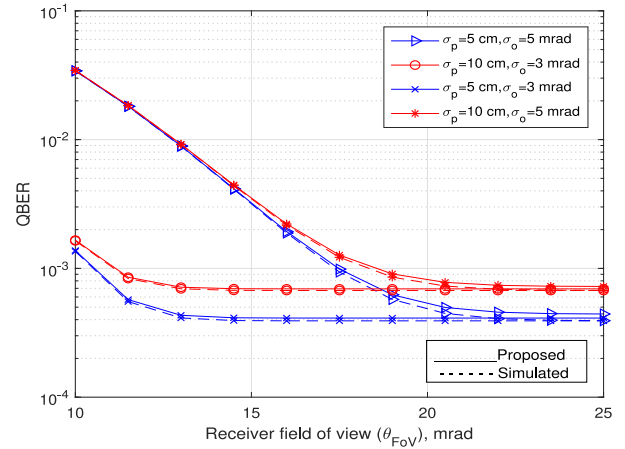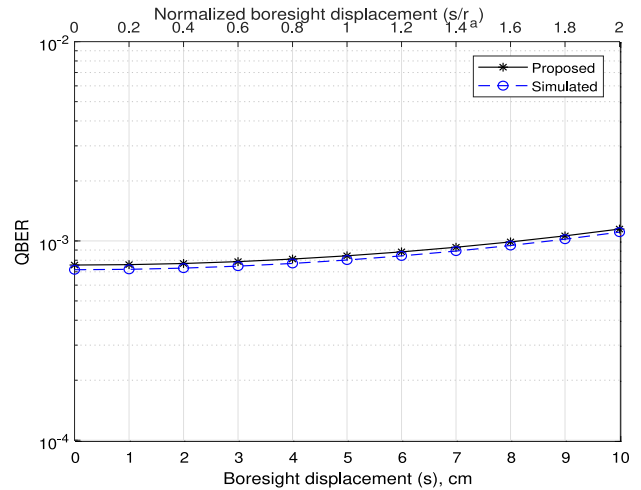
and is kept below the QBER$_{\mathrm{th}}$ of 10^{-3} confirming the validity of optimizing the receiver's θ_{FoV} to 20 mrad.

The boresight displacement is another parameter that should be calculated in order to keep the QBER below 10^{-3}. Given the optimized values of the parameters previously studied, $\mathrm{P}_T = 4$ dBm, $\theta_{\mathrm{FoV}} = 20$ mrad, and $\theta_{\mathrm{div}} = 1.5$ mrad Fig. 8 shows the effect of changing boresight displacement on the QBER. It is clear to see that the system tolerates boresight displacement up to 7 cm while maintaining the QBER below the threshold value.

Fig. 9 is shown to illustrate the effect of optimized parameter values (θ_{FoV}=20 mrad and θ_{div}=1.5 mrad) on the outage probability. It can be seen that, the outage probability reaches the dedicated threshold (10^{-2}) at $\mathrm{P}_T > 3$ dBm for SNR$_{\mathrm{th}}$ = 5 dB. Furthermore, for $\mathrm{P}_T = 4$ dBm the SNR$_{\mathrm{th}}$ must not be more than 6.5 dB in order to keep the outage probability below the desired threshold.

The RKR and SKR as a function of the transmit power are represented in Fig. 10 for different mean value of channel transmittance $\langle T \rangle$. $\mathrm{P}_T = 4$ dBm results in an RKR of 7.2 and 11 b/s/Hz for $\langle T \rangle = 0.6$ and 0.9, respectively. Also, the results
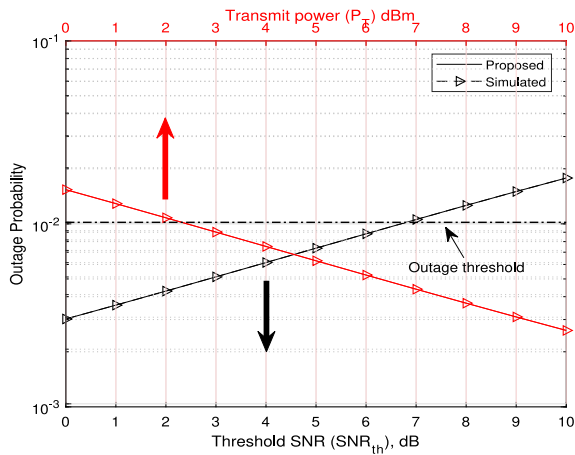
Fig. 9. Outage probability versus the transmit power at SNR_{th}= 5 dB and versus SNR_{th} at θ_{div}=1.5 mrad, and θ_{Fov}=20 mrad for σ_p=10 cm, σ_o=5 mrad.
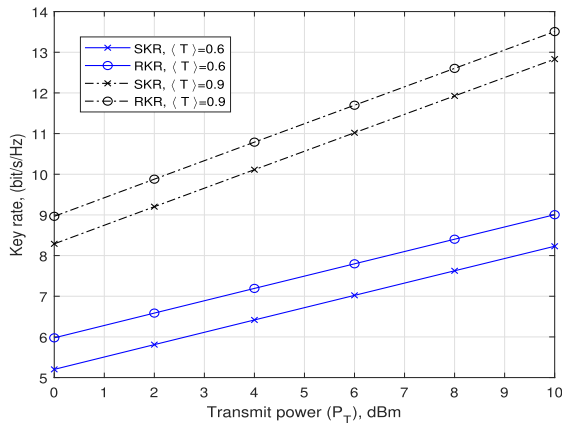

Fig. 10. SKR and RKR versus transmit power as a function of the mean channel transmittance for θ_{div}=1.5 mrad, and θ_{Fov}=20 mrad.

give a SKR of 6.4 and 10 b/s/Hz for $\langle T \rangle = 0.6$ and 0.9, respectively.

VI. CONCLUSION

This paper introduces a comprehensive study of an integrated system that gains the benefits of UAVs, FSO links, and CV-QKD protocols. The proposed system is a UAV-based FSO system utilizing DP-QPSK modulation and prepare and measure CV-QKD protocol based on GMCS under collective attack. The study included the system design, performance evaluation, parameter optimization, and security analysis while considering the combined effects of critical parameters such as excess noise, channel fluctuating transmittance, different atmospheric effects, UAV's position deviation, detection efficiency, and collective attack. The closed-form expressions for QBER and outage probability are driven. The asymptotic RKR and SKR expressions are given considering the atmospheric channel PDF. In order to achieve QBER $< 10^{-3}$ and outage probability $< 10^{-2}$, it is found that the optimum receiver's field of view, beam's divergence angle, transmit power are 20 mrad, 1.5 mrad, and 4 dBm, respectively. Furthermore, the RKR and SKR are 6.4 and 10 at mean channel transmittance of 0.6 and increase to 7.2 and 11 if the transmittance reaches 0.9. These optimized values

enable the proposed system to tolerate boresight displacement up to 7 cm while satisfying the design criteria. The Monte Carlo simulation is used to verify the analytical results and closed-form expressions. Apart from the standard security requirements, the proposed system achieves perfect secrecy and non-repudiation, which are essential to secure military applications, financial sector transactions, and critical information systems. Moreover, the CV-QKD with multiple antennas will be further investigated in future research.

REFERENCES

[1] N. Alshaer, T. Ismail, and M. E. Nasr, "Enhancing earth-to-satellite FSO system spectrum efficiency with adaptive M-ary PSK and SIMO in presence of scintillation and beam wander," *AEU- Int. J. Electron. Commun.*, vol. 125, pp. 1–9, 2020.

[2] J. D. Morris, M. R. Grimaila, D. D. Hodson, D. Jacques, and G. Baumgartner, "A survey of quantum key distribution (QKD) technologies," in *Emerging Trends in ICT Security*. Amsterdam, The Netherlands: Elsevier, 2014, pp. 141–152.

[3] B. Korzh *et al.*, "Provably secure and practical quantum key distribution over 307 km of optical fibre," *Nature Photon.*, vol. 9, no. 3, pp. 163–168, 2015.

[4] T. Schmitt-Manderbach *et al.*, "Experimental demonstration of free-space decoy-state quantum key distribution over 144 km," *Phys. Rev. Lett.*, vol. 98, no. 1, pp. 1–4, 2007.

[5] T. Ismail, E. Leitgeb, Z. Ghassemlooy, and M. Al-Nahhal, "Performance improvement of FSO system using multi-pulse pulse position modulation and SIMO under atmospheric turbulence conditions and with pointing errors," *IET Netw.*, vol. 7, no. 4, pp. 165–172, 2018.

[6] N. Alshaer, T. Ismail, H. Seleem, and M. E. Nasr, "Optimized beam size of optical ground-to-satellite link over turbulence and beam-wandering," in *Proc. 21st Int. Conf. Transparent Opt. Netw.*, 2019, pp. 1–4.

[7] M. Niu, J. Cheng, J. F. Holzman, and L. McPhail, "Performance analysis of coherent free space optical communication systems with k-distributed turbulence," in *Proc. IEEE Int. Conf. Commun.*, 2009, pp. 1–5.

[8] L. Li *et al.*, "Free-space optical communication using coherent detection and double adaptive detection thresholds," *IEEE Photon. J.*, vol. 11, no. 1, Feb. 2019, Art. no. 7900217.

[9] K. Roberts *et al.*, "Performance of dual-polarization QPSK for optical transport systems," *J. Lightw. Technol.*, vol. 27, no. 16, pp. 3546–3559, 2009.

[10] G. P. Agrawal, *Fiber-Optic Communication Systems*. Hoboken, NJ, USA: Wiley, 2012.

[11] M. Aljehani, M. Inoue, A. Watanbe, T. Yokemura, F. Ogyu, and H. Iida, "UAV communication system integrated into network traversal with mobility," *SN Appl. Sci.*, vol. 2, pp. 1–20, 2020.

[12] M. Aljehani and M. Inoue, "Safe map generation after a disaster, assisted by an unmanned aerial vehicle tracking system," *IEEJ Trans. Elect. Electron. Eng.*, vol. 14, no. 2, pp. 271–282, 2019.

[13] Y. Zeng, R. Zhang, and T. J. Lim, "Wireless communications with unmanned aerial vehicles: Opportunities and challenges," *IEEE Commun. Mag.*, vol. 54, no. 5, pp. 36–42, May 2016.

[14] "fsona.com," Accessed: Jun. 4, 2021. [Online]. Available: http://fsona.com/product.php?sec=safety/

[15] "cablefree.net," Accessed: Jun. 4, 2021. https://www.cablefree.net/

[16] A. Jurado-Navas, J. M. Garrido-Balsells, J. F. Paris, A. Puerta-Notario, and J. Awrejcewicz, "A unifying statistical model for atmospheric optical scintillation," in *Proc. Numer. Simul. Phys. Eng. Process.*, 2011, vol. 181, pp. 1–4.

[17] A. A. Farid and S. Hranilovic, "Outage capacity optimization for free-space optical links with pointing errors," *J. Lightw. Technol.*, vol. 25, no. 7, pp. 1702–1710, 2007.

[18] A. Kaadan, H. H. Refai, and P. G. LoPresti, "Multielement FSO transceivers alignment for inter-UAV communications," *J. Lightw. Technol.*, vol. 32, no. 24, pp. 4785–4795, 2014.

[19] M. Li, Y. Hong, C. Zeng, Y. Song, and X. Zhang, "Investigation on the UAV-to-satellite optical communication systems," *IEEE J. Sel. Areas Commun.*, vol. 36, no. 9, pp. 2128–2138, Sep. 2018.

[20] L. Li *et al.*, "High-capacity free-space optical communications between a ground transmitter and a ground receiver via a UAV using multiplexing of multiple orbital-angular-momentum beams," *Sci. Rep.*, vol. 7, no. 1, pp. 1–12, 2017.

[21] M. T. Dabiri, S. M. S. Sadough, and M. A. Khalighi, "Channel modeling and parameter optimization for hovering UAV-based free-space optical links," *IEEE J. Sel. Areas Commun.*, vol. 36, no. 9, pp. 2104–2113, Sep. 2018.

[22] M. T. Dabiri, S. M. S. Sadough, and I. S. Ansari, "Tractable optical channel modeling between UAVs," *IEEE Trans. Veh. Technol.*, vol. 68, no. 12, pp. 11543–11550, Dec. 2019.

[23] S. Khankalantary, M. T. Dabiri, and H. Safi, "BER performance analysis of drone-assisted optical wireless systems with APD receiver," *Opt. Commun.*, vol. 463, pp. 1–7, 2020.

[24] P. V. Trinh, T. V. Pham, N. T. Dang, H. V. Nguyen, S. X. Ng, and A. T. Pham, "Design and security analysis of quantum key distribution protocol over free-space optics using dual-threshold direct-detection receiver," *IEEE Access*, vol. 6, pp. 4159–4175, 2018.

[25] P. Papanastasiou, C. Weedbrook, and S. Pirandola, "Continuous-variable quantum key distribution in uniform fast-fading channels," *Phys. Rev. A*, vol. 97, no. 3, pp. 1–7, 2018.

[26] N. Hosseinidehaj, Z. Babar, R. Malaney, S. X. Ng, and L. Hanzo, "Satellite-based continuous-variable quantum communications: State-of-the-art and a predictive outlook," *IEEE Commun. Surv. Tut.*, vol. 21, no. 1, pp. 881–919, Jan.–Mar. 2019.

[27] C. Weedbrook *et al.*, "Gaussian quantum information," *Rev. Modern Phys.*, vol. 84, no. 2, pp. 621–672, 2012.

[28] F. Grosshans, G. Van Assche, J. Wenger, R. Brouri, N. J. Cerf, and P. Grangier, "Quantum key distribution using Gaussian-modulated coherent states," *Nature*, vol. 421, no. 6920, pp. 238–241, 2003.

[29] N. J. Cerf, M. Levy, and G. Van Assche, "Quantum distribution of Gaussian keys using squeezed states," *Phys. Rev. A*, vol. 63, no. 5, pp. 1–5, 2001.

[30] R. García-Patrón and N. J. Cerf, "Continuous-variable quantum key distribution protocols over noisy channels," *Phys. Rev. Lett.*, vol. 102, no. 13, pp. 1–4, 2009.

[31] A. Semenov, F. Töppel, D. Y. Vasylyev, H. Gomonay, and W. Vogel, "Homodyne detection for atmosphere channels," *Phys. Rev. A*, vol. 85, no. 1, pp. 1–9, 2012.

[32] F. Grosshans and P. Grangier, "Continuous variable quantum cryptography using coherent states," *Phys. Rev. Lett.*, vol. 88, no. 5, pp. 1–6, 2002.

[33] Y. Zhang *et al.*, "Continuous-variable QKD over 50 km commercial fiber," *Quantum Sci. Technol.*, vol. 4, no. 3, pp. 1–19, 2019.

[34] T. Wang *et al.*, "High key rate continuous-variable quantum key distribution with a real local oscillator," *Opt. Exp.*, vol. 26, no. 3, pp. 2794–2806, 2018.

[35] M. Navascués, F. Grosshans, and A. Acin, "Optimality of Gaussian attacks in continuous-variable quantum cryptography," *Phys. Rev. Lett.*, vol. 97, no. 19, pp. 1–4, 2006.

[36] P. Huang, J. Huang, Z. Zhang, and G. Zeng, "Quantum key distribution using basis encoding of Gaussian-modulated coherent states," *Phys. Rev. A*, vol. 97, no. 4, 2018, Art. no. 042311.

[37] C. Quintana *et al.*, "Low size, weight and power quantum key distribution system for small form unmanned aerial vehicles," in *Proc. Free-Space Laser Commun.*, vol. 10910. Bellingham, WA, USA: SPIE, 2019, pp. 1–5.

[38] N. Alshaer, T. Ismail, and M. E. Nasr, "Performance evaluation and security analysis of ground-to-satellite FSO system with CV-QKD protocol," *IET Commun.*, vol. 14, no. 10, pp. 1534–1542, 2020.

[39] H.-Y. Liu *et al.*, "Drone-based entanglement distribution towards mobile quantum networks," *Nat. Sci. Rev.*, vol. 7, no. 5, pp. 921–928, 2020.

[40] H.-Y. Liu *et al.*, "Optical-relayed entanglement distribution using drones as mobile nodes," *Phys. Rev. Lett.*, vol. 126, no. 2, pp. 1–6, 2021.

[41] N. Alshaer, A. Moawad, and T. Ismail, "Reliability and security analysis of an entanglement-based QKD protocol in a dynamic ground-to-UAV FSO communications system," *IEEE Access*, vol. 9, pp. 168052–168067, 2021.

[42] I. Kaminow, T. Li, and A. E. Willner, *Optical Fiber Telecommunications VB: Systems and Networks*. Amsterdam, The Netherlands: Elsevier, 2010.

[43] H. G. Sandalidis, T. A. Tsiftsis, and G. K. Karagiannidis, "Optical wireless communications with heterodyne detection over turbulence channels with pointing errors," *J. Lightw. Technol.*, vol. 27, no. 20, pp. 4440–4445, 2009.

[44] C. C. Chan, *Optical Performance Monitoring: Advanced Techniques for Next-Generation Photonic Networks*. New York, NY, USA: Academic, 2010.

[45] A. E. Morra, H. S. Khallaf, H. M. Shalaby, and Z. Kawasaki, "Performance analysis of both shot-and thermal-noise limited multipulse PPM receivers in gamma-gamma atmospheric channels," *J. Lightw. Technol.*, vol. 31, no. 19, pp. 3142–3150, 2013.

[46] N. Alshaer, T. Ismail, and M. E. Nasr, "Generic evaluation of FSO system over Málaga turbulence channel with MPPM and non-zero-boresight pointing errors," *IET Commun.*, vol. 14, no. 18, pp. 3294–3302, 2020.

[47] K. Zhong, X. Zhou, J. Huo, C. Yu, C. Lu, and A. P. T. Lau, "Digital signal processing for short-reach optical communications: A review of current technologies and future trends," *J. Lightw. Technol.*, vol. 36, no. 2, pp. 377–400, 2018.

[48] H. Li *et al.*, "An accurate and robust PDL monitor by digital signal processing in coherent receiver," in *Proc. Opt. Fiber Commun. Conf. Expo.*, 2018, pp. 1–3.

[49] R. Miglani and J. S. Malhotra, "Performance enhancement of high-capacity coherent DWDM free-space optical communication link using digital signal processing," *Photonic Netw. Commun.*, vol. 38, no. 3, pp. 326–342, 2019.

[50] S. Kartalopoulos, *Free Space Optical Networks for Ultra-Broad Band Services*. Hoboken, NJ, USA: Wiley, 2011.

[51] K. Anbarasi, C. Hemanth, and R. Sangeetha, "A review on channel models in free space optical communication systems," *Opt. Laser Technol.*, vol. 97, pp. 161–171, 2017.

[52] P. Beckmann and A. Spizzichino, *The Scattering of Electromagnetic Waves From Rough Surfaces*. London, U.K.; Norwood, Massachusetts, USA:Artech House. 1987.

[53] F. Yang, J. Cheng, and T. A. Tsiftsis, "Free-space optical communication with nonzero boresight pointing errors," *IEEE Trans. Commun.*, vol. 62, no. 2, pp. 713–725, Feb. 2014.

[54] K. Kiasaleh, "Channel estimation for FSO channels subject to gamma-gamma turbulence," in *Proc. Int. Conf. Space Opt. Syst. Appl.*, 2012, pp. 1–7.

[55] S. Wang, P. Huang, T. Wang, and G. Zeng, "Atmospheric effects on continuous-variable quantum key distribution," *New J. Phys.*, vol. 20, no. 1, pp. 1–19, 2018.

[56] Y. Guo, C. Xie, Q. Liao, W. Zhao, G. Zeng, and D. Huang, "Entanglement-distillation attack on continuous-variable quantum key distribution in a turbulent atmospheric channel," *Phys. Rev. A*, vol. 96, Aug. 2017, Art. no. 022320. [Online]. Available: https://link.aps.org/doi/10.1103/PhysRevA.96.022320

[57] Y. Zheng, P. Huang, T. Wang, J. Peng, Z. Cao, and G. Zeng, "The improvement of performance for continuous-variable quantum key distribution with imperfect Gaussian modulation," *Int. J. Theor. Phys.*, vol. 58, no. 11, pp. 3414–3435, 2019.

[58] I. Derkach, V. C. Usenko, and R. Filip, "Squeezing-enhanced quantum key distribution over atmospheric channels," *New J. Phys.*, vol. 22, no. 5, pp. 1–11, 2020.

[59] G. Chai, Z. Cao, W. Liu, S. Wang, P. Huang, and G. Zeng, "Parameter estimation of atmospheric continuous-variable quantum key distribution," *Phys. Rev. A*, vol. 99, no. 3, pp. 1–12, 2019.

[60] S. Fossier, E. Diamanti, T. Debuisschert, R. Tualle-Brouri, and P. Grangier, "Improvement of continuous-variable quantum key distribution systems by using optical preamplifiers," *J. Phys. B: Atomic, Mol. Opt. Phys.*, vol. 42, no. 11, pp. 1–11, 2009.

[61] F. Laudenbach *et al.*, "Continuous-variable quantum key distribution with Gaussian modulation-the theory of practical implementations," *Adv. Quantum Technol.*, vol. 1, no. 1, pp. 1–37, 2018.

[62] J. G. Proakis and M. Salehi, *Digital Communications*. New York, USA, McGraw-Hill, 2001.

[63] "wolfram.functions," Accessed: Mar. 15, 2021. http://functions.wolfram.com/HypergeometricFunctions/MeijerG/21/02/03/01/

[64] M. Al-Nahhal and T. Ismail, "Enhancing spectral efficiency of FSO system using adaptive SIM/M-PSK and SIMO in the presence of atmospheric turbulence and pointing errors," *Int. J. Commun. Syst.*, vol. 32, no. 9, pp. 1–13, 2019.